Effective Local Permittivity Model for Nonlocal Wire Media

Alexander B. Yakovlev, *Senior Member, IEEE*, Mário G. Silveirinha, *Fellow, IEEE*, and George W. Hanson, *Fellow, IEEE*

***Abstract*—A local permittivity model is proposed to accurately characterize spatial dispersion (SD) in nonlocal wire medium (WM) structures with arbitrary terminations. A closed-form expression for the local thickness-dependent permittivity is derived for a general case of a bounded WM with lumped impedance insertions and terminated with impedance surfaces, which takes into account the effects of SD and loads/terminations in the averaged sense per length of the wire medium. The proposed approach results in a local model formalism and accurately predicts the response of WM structures for near-field and far-field excitation. It is also shown that a traditional transmission network and circuit model can be effectively used to quantify the interaction of propagating and evanescent waves with WM structures. In addition, the derived analytical expression for the local thickness-dependent permittivity has been used in the full-wave numerical solver (CST Microwave Studio) demonstrating a drastic reduction in the computation time and memory in the solution of near-field and far-field problems involving wire media.**

***Index Terms*—Additional boundary condition (ABC), circuit model, homogenization theory, metamaterials, spatial dispersion (SD), wire medium (WM).**

I. INTRODUCTION

SPATIAL dispersion (SD) of continuous materials, or homogenized materials with effective material parameters, characterizes the dependence of constitutive parameters on wavevector, such that the constitutive relations between the macroscopic fields and electric/magnetic dipole moment are nonlocal [1], [2]. Nonlocal effects generate extra propagating or evanescent waves which in case of wire medium (WM) can be viewed as extraordinary waves. The wave-matter interaction in bounded nonlocal materials is typically modeled by expanding the field in terms of the waves of unbounded domains, and then imposing the usual boundary conditions as well as additional boundary conditions (ABCs) at material interfaces. The ABCs are needed to account for the extra waves present in nonlocal materials [3], [4].

In this article, we focus on the analysis of electromagnetic interactions with bounded WM structures. It is already well known that wire media exhibits strong SD at microwave frequencies, even for very long wavelengths [5], [6]. The role of SD effects has been addressed [7]–[10], and it has been shown that the nonlocal homogenization formalism is essential in the solution of scattering, radiation, and excitation problems involving WM-type structures [8], [9], [11]–[24]. In this regard, the methodology proposed in [25] is of particular interest, wherein the nonlocal susceptibility of the bounded homogenized WM in the spatial transform-domain is given by the Green's function for the same geometric region subject to ABCs at the wire-end terminations [26]–[29]. Based on the nonlocal formalism for bounded WM proposed in [25], a local thickness-dependent permittivity has been derived in closed form for a grounded WM and symmetric WM terminated with impedance surfaces at the wire connections [30]. It was shown that the local permittivity that accounts for SD must depend on the thickness of the WM slab and on the termination of the wires ([31] discusses the dependence of effective material parameters on geometric metamaterial parameters).

In recent work [32], it is shown that the spatial nonlocality in metals can be effectively modeled by a composite material comprising a thin local dielectric layer on top of a local metal, such that the nonlocal effects are captured in a deeply subwavelength effective dielectric layer. In general, this is not the case with WM, wherein the nonlocal effects are distributed throughout the entire structure due to the presence of two extraordinary waves: transverse magnetic (TM), which is evanescent below the plasma frequency, and transverse electromagnetic (TEM), which propagates in WM as in a uniaxial material with extreme anisotropy.

Here, we generalize the concepts developed in [25], [30], [33], and [34] to the case of WM slab with lumped impedance insertions (including the case of p-i-n diodes at the wire connections) and terminated with different impedance surfaces at the top and bottom WM interfaces. A local thickness-dependent permittivity is derived in closed form, and takes into account SD and the effect of the loads/terminations in the averaged sense per thickness of the WM slab. The local thickness-dependent permittivity for an asymmetric configuration with lumped impedance insertions and terminated with arbitrary impedance surfaces first appeared in [35], and here the theory is verified with full-wave results, and several other geometries/examples have been added.

Manuscript received June 4, 2019; revised August 21, 2019; accepted October 25, 2019. Date of publication November 22, 2019; date of current version April 7, 2020. This work was supported in part by (M.S.) through the Fundação para Ciência e a Tecnologia (FCT) under Project UID/EEA/50008/2019, and in part by the European Regional Development Fund (FEDER), through the Competitiveness and Internationalization Operational Programme under Grant COMPETE 2020 of the Portugal 2020 framework, under Project, RETIOT, POCI-01-0145 FEDER-016432. *(Corresponding author: Alexander B. Yakovlev.)*

A. B. Yakovlev is with the Department of Electrical Engineering, The University of Mississippi, Oxford, MS 38677-1848 USA (e-mail: yakovlev@olemiss.edu).

M. G. Silveirinha is with the Instituto Superior Técnico, University of Lisbon, 1049-001 Lisbon, Portugal, and also with the Instituto de Telecomunicações, 1049-001 Lisbon, Portugal (e-mail: mario.silveirinha@co.it.pt).

G. W. Hanson is with the Department of Electrical Engineering and Computer Science, University of Wisconsin–Milwaukee, Milwaukee, WI 53211 USA (e-mail: george@uwm.edu).

Color versions of one or more of the figures in this article are available online at http://ieeexplore.ieee.org.

Digital Object Identifier 10.1109/TAP.2019.2951129

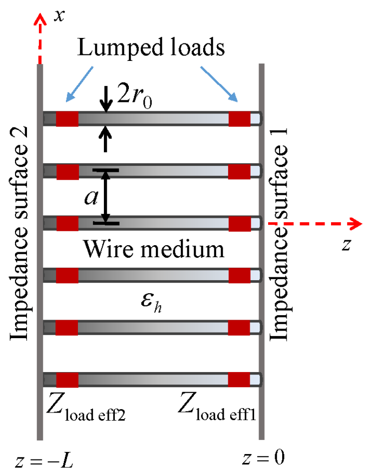

Fig. 1. Geometry of a 2-D WM structure with the wires connected to impedance surfaces through lumped impedance insertions.

This article is organized as follows. In Section II, we introduce the formalism of the nonlocal susceptibility/permittivity in the spatial domain for a WM slab with lumped loads/impedance surfaces terminations, and derive a closed-form expression for the local thickness-dependent permittivity. Also, a transmission network approach and a circuit model are discussed. In Section III, various numerical examples in the local framework are demonstrated and the results are compared with the nonlocal solution and full-wave numerical simulations. Section IV summarizes the main results and conclusions. An appendix provides analytical details of the Green's function problem. A time dependence of the form $e^{j\omega t}$ is assumed and suppressed.

II. Local Thickness-Dependent Permittivity of WM

Consider a WM structure with the geometry shown in Fig. 1. The structure is comprised by a 2-D lattice of z-directed thin metallic wires of thickness L connected through lumped impedance insertions to impedance surfaces at the wire-end interfaces at $z=0$ and $z=-L$. For simplicity, we assume air semi-infinite regions external to the structure. The period of wires is a, the radius of wires is r_0, and the relative permittivity of the host medium is ε_h. The impedance surfaces are characterized by the surface admittance, $\bar{\mathbf{Y}}_{g1,2} = (\hat{\mathbf{x}}\hat{\mathbf{x}}+\hat{\mathbf{y}}\hat{\mathbf{y}})Y_{g1,2}$, with the closed-form expressions for periodic printed (capacitive) or slotted (inductive) subwavelength grids presented in [36]. The lumped impedance insertions are given in terms of the effective load impedance, $Z_{\text{load eff1,2}}$ [23], [28], [37].

According to [25], the nonlocal response for the geometry in Fig. 1 that accounts for a material boundary in the spatial transform-domain satisfies the following system of equations written from a macroscopic perspective for a homogenized WM

$$\nabla\times\mathbf{E} = -j\omega\mu\mathbf{H} \tag{1}$$

$$\nabla\times\mathbf{H} = (\bar{\mathbf{Y}}_{g1}\delta(z)+\bar{\mathbf{Y}}_{g2}\delta(z+L))\cdot\mathbf{E}+j\omega P_z^{\text{cond}}\hat{\mathbf{z}}+j\omega\varepsilon_0\varepsilon_h\mathbf{E} \tag{2}$$

$$\left(k_h^2+\frac{\partial^2}{\partial z^2}\right)P_z^{\text{cond}} = -k_p^2\varepsilon_0\varepsilon_h E_z \tag{3}$$

where P_z^{cond} is the conductive polarization due to the z-directed WM

$$P_z^{\text{cond}}(z) = \varepsilon_0\int_{-L}^{0}\chi^{\text{cond}}(z,z')E_z(z')dz'. \tag{4}$$

Here, the susceptibility χ^{cond} determines the nonlocal response for the uniaxial WM that accounts for the material interface. It is proportional to the Green's function associated with (3) subject to the ABCs at the interfaces, such that $\chi^{\text{cond}}(z,z') = \varepsilon_h k_p^2 g(z,z')$. The Green's function problem for the geometry in Fig. 1 is presented in the appendix. From (1) to (3), $k_h = k_0\sqrt{\varepsilon_h}$ is the wavenumber of the host medium, and k_p is the plasma wavenumber defined by $(k_p a)^2 \approx 2\pi/(\ln(a/(2\pi r_0))+0.5275)$ [6].

The nonlocal permittivity for WM can be described in terms of a Green's function, $g(z,z')$, which takes into account the material SD and the effect of the lumped loads and the material boundaries (see Fig. 1)

$$\varepsilon_{\text{nonloc}}(z,z') = \varepsilon_h k_p^2 g(z,z')+\varepsilon_h\delta(z-z'). \tag{5}$$

With the known Green's function (see Appendix) the nonlocal permittivity (5) can be approximated by a local response, $\varepsilon_{\text{nonloc}}(z,z')\approx\varepsilon_{\text{loc}}\delta(z-z')$, where ε_{loc} is the *local thickness-dependent permittivity* [30] for a WM structure of thickness L with the wires connected to impedance surfaces through lumped loads (see Fig. 1) resulting in

$$\begin{aligned}\varepsilon_{\text{loc}} &= \frac{1}{L}\int_{-L}^{0}\int_{-L}^{0}\varepsilon_{\text{nonloc}}(z,z')dzdz'\\ &= \frac{\varepsilon_h k_p^2}{L}\int_{-L}^{0}\int_{-L}^{0}g(z,z')dzdz'+\varepsilon_h.\end{aligned} \tag{6}$$

Equation (5) is an exact relation, and by representing $\varepsilon_{\text{nonloc}}(z,z')\approx\varepsilon_{\text{loc}}\delta(z-z')$, we assume that the material response in a WM slab is localized. This may happen either because the SD of the medium is weak (which evidently is not the case of the WM), or, alternatively, because the material boundaries effectively localize the response to a spatial region with thickness L. The latter is the mechanism relevant in our system.

Performing the double integral (6) with the Green's function in (19) and (20), a closed-form expression of the local thickness-dependent permittivity for a general case presented in Fig. 1 can be obtained

$$\begin{aligned}\varepsilon_{\text{loc}} &= \varepsilon_h\left(1-\frac{k_p^2}{k_h^2}\right)\\ &\quad+\varepsilon_h\frac{k_p^2}{Lk_h^3}\frac{2-2\cos(k_hL)+k_h(\alpha_1+\alpha_2)\sin(k_hL)}{(1-k_h^2\alpha_1\alpha_2)\sin(k_hL)+k_h(\alpha_1+\alpha_2)\cos(k_hL)}\end{aligned} \tag{7}$$

where α_1 and α_2 are defined in the appendix for different cases of wire-end terminations. The first term in (7) is the usual local permittivity of a bulk WM (Drude permittivity), and the second thickness-dependent term takes into account SD in the WM in the averaged sense per thickness L and the effect of the loads/boundaries and the interaction between the boundaries. In a few limiting cases, the obtained expression (7)

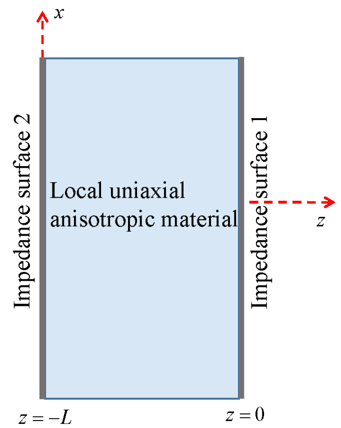

Fig. 2. Local uniaxial anisotropic material with impedance surfaces at the interfaces as an equivalent geometry to the WM structure presented in Fig. 1.

simplifies to those presented in [30], such that for a grounded WM slab with impedance surface at $z = 0$ ($\alpha_1 = \alpha, \alpha_2 \to \infty$), we obtain the expression in [30, eq. (16)], and for a grounded WM slab with open-end wires (no impedance surface at $z = 0$ ($\alpha_1 = 0, \alpha_2 \to \infty$)) (7) results in [30, eq. (17)]. Also, it can be verified that the limiting cases to symmetric structures (two-sided WM slab with identical impedance surfaces, $\alpha_1 = \alpha_2 = \alpha$, and the WM slab with open-end wires, $\alpha_1 = \alpha_2 = 0$) are also satisfied resulting in [30, eqs. (16) and (17)] by changing L to $L/2$ in the obtained expressions.

The closed-form expression (7) for a local thickness-dependent permittivity can be used in the analysis of various near-field and far-field electromagnetic problems formulated on a local framework

$$\nabla \times \mathbf{H} = j\omega\varepsilon_0 \bar{\boldsymbol{\varepsilon}}_{\text{total}}(z) \cdot \mathbf{E}(z) \tag{8}$$

where

$$\bar{\boldsymbol{\varepsilon}}_{\text{total}}(z) = \frac{1}{j\omega\varepsilon_0}(\bar{\mathrm{Y}}_{g1}\delta(z) + \bar{\mathrm{Y}}_{g2}\delta(z+L)) + \varepsilon_{\text{loc}}\hat{\mathbf{z}}\hat{\mathbf{z}} + \varepsilon_h(\hat{\mathbf{x}}\hat{\mathbf{x}} + \hat{\mathbf{y}}\hat{\mathbf{y}}). \tag{9}$$

The scattering problem for the geometry shown in Fig. 1 with the WM slab (including the lumped loads) replaced by the local uniaxial anisotropic material shown in Fig. 2 with the host permittivity ε_h in the x- and y-directions and the thickness-dependent permittivity (7) in the z-direction can be formulated in a local framework. We assume the TM-polarized plane wave is obliquely incident on the structure from the air region with $z > 0$. The plane wave is characterized by H_y, E_x, and E_z components, and the magnetic field in the air regions and in the WM slab can be expressed as follows:

$$H_y = \begin{cases} e^{\gamma_0 z} - \rho e^{-\gamma_0 z}, & z > 0 \\ A^+ e^{\gamma_{\text{loc}} z} + A^- e^{-\gamma_{\text{loc}} z}, & -L \le z \le 0 \\ T e^{\gamma_0 (z+L)}, & z < -L \end{cases} \tag{10}$$

where ρ and T are the reflection and transmission coefficients, respectively, $\gamma_0 = \sqrt{k_x^2 - k_0^2}$, $\gamma_{\text{loc}} = \sqrt{(\varepsilon_h k_x^2/\varepsilon_{\text{loc}}) - k_h^2}$ [30], and k_x is the $x-$component of the wavevector $\mathbf{k} = (k_x, 0, k_z)$.

By imposing the usual boundary conditions for tangential electric-field and magnetic-field components at the interfaces at $z = 0$ and $z = -L$, the following system of linear equations is obtained

$$\begin{pmatrix} \varepsilon_h\gamma_0 & -\gamma_{\text{loc}} & \gamma_{\text{loc}} & 0 \\ 1+\dfrac{\gamma_0}{j\omega\varepsilon_0}Y_{g1} & 1 & 1 & 0 \\ 0 & \gamma_{\text{loc}}e^{-\gamma_{\text{loc}}} & -\gamma_{\text{loc}}e^{\gamma_{\text{loc}}} & -\varepsilon_h\gamma_0 \\ 0 & e^{-\gamma_{\text{loc}}} & e^{\gamma_{\text{loc}}} & -1-\dfrac{\gamma_0}{j\omega\varepsilon_0}Y_{g2} \end{pmatrix} \times \begin{pmatrix} \rho \\ A^+ \\ A^- \\ T \end{pmatrix} = \begin{pmatrix} -\varepsilon_h\gamma_0 \\ 1-\dfrac{\gamma_0}{j\omega\varepsilon_0}Y_{g1} \\ 0 \\ 0 \end{pmatrix} \tag{11}$$

which can be solved for the unknown coefficients ρ, T, and $A^{\pm}$.

Also, for the geometry in Fig. 1 with the local thickness-dependent permittivity (7) for a WM slab (with the equivalent problem shown in Fig. 2) the transmission network (ABCD matrix) can be easily obtained

$$\begin{bmatrix} A & B \\ C & D \end{bmatrix} = \begin{bmatrix} 1 & 0 \\ Y_{g2} & 1 \end{bmatrix} \times \begin{bmatrix} \cosh(\gamma_{\text{loc}}L) & Z_{\text{loc}}\sinh(\gamma_{\text{loc}}L) \\ \dfrac{1}{Z_{\text{loc}}}\sinh(\gamma_{\text{loc}}L) & \cosh(\gamma_{\text{loc}}L) \end{bmatrix} \times \begin{bmatrix} 1 & 0 \\ Y_{g1} & 1 \end{bmatrix} \tag{12}$$

where $Z_{\text{loc}} = (\gamma_{\text{loc}}/j\omega\varepsilon_0\varepsilon_h)$ is the characteristic impedance of the WM slab as the transmission line with the local thickness-dependent permittivity (7). The reflection and transmission coefficients (S-parameters) are retrieved from the ABCD-matrix parameters with the known expressions from the microwave engineering [38, p. 192; with Z_0 replaced by Z_{loc}]. Obviously, in a local framework the transmission network (12) (with conversion to the S-parameters) and the field approach (11) give the same results for ρ and T.

For a symmetric WM structure with respect to the impedance surface terminations, $Y_{g1} = Y_{g2} = Y_g$, even though the lumped impedance insertions can be different and in general $\alpha_1 \neq \alpha_2$, a simple circuit model with even and odd excitations (corresponding to the symmetry of the structure by a perfect electric conductor (PEC) and perfect magnetic conductor (PMC), respectively, placed at the center of the structure) can be obtained [39]

$$\rho_e = \frac{Y_0 - Y_g - Y_{\text{loc}}\coth\left(\gamma_{\text{loc}}\frac{L}{2}\right)}{Y_0 + Y_g + Y_{\text{loc}}\coth\left(\gamma_{\text{loc}}\frac{L}{2}\right)} \tag{13}$$

$$\rho_o = \frac{Y_0 - Y_g - Y_{\text{loc}}\tanh\left(\gamma_{\text{loc}}\frac{L}{2}\right)}{Y_0 + Y_g + Y_{\text{loc}}\tanh\left(\gamma_{\text{loc}}\frac{L}{2}\right)} \tag{14}$$

where $Y_{\text{loc}} = 1/Z_{\text{loc}}$ and $Y_0 = j\omega\varepsilon_0/\gamma_0$. The reflection/transmission response of the entire WM structure is obtained by the superposition principle as $\rho = (\rho_e + \rho_o)/2$ and $T = (\rho_e - \rho_o)/2$.

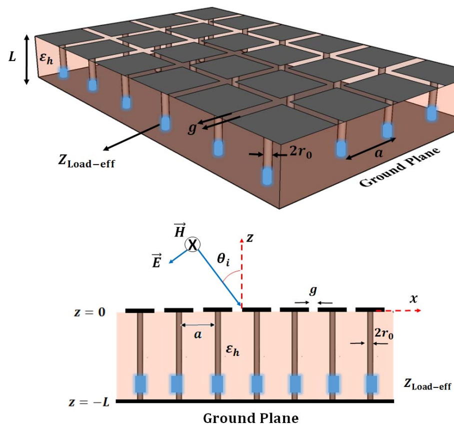

Fig. 3. Geometry of a mushroom high-impedance surface with loaded vias with an obliquely incident TM-polarized plane wave.

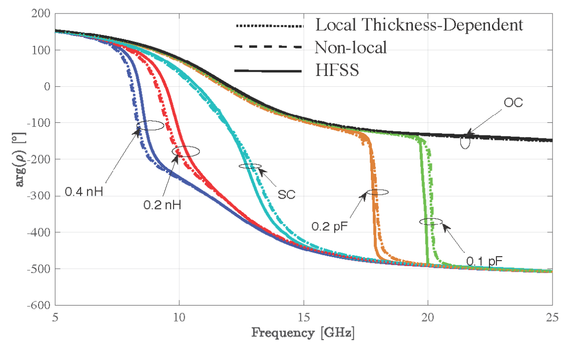

Fig. 4. Phase of the reflection coefficient for a mushroom structure with the vias connected to the ground through inductive and capacitive loads (including the cases of SC and OC). The dimensions of the structure are: $a = 2$ mm, $g = 0.2$ mm, $r_0 = 0.05$ mm, $L = 1$ mm, $\varepsilon_h = 10.2$, and $\theta_i = 60°$. The load is connected to the ground through a gap of 0.1 mm with the parasitic capacitance $C_{\text{par}} \approx 0.02$ pF and parasitic inductance $L_{\text{par}} \approx 0.06$ nH (estimated by curve fitting).

We should point out that the geometry in Fig. 1 serves as a building block and with the obtained local thickness-dependent permittivity (7) it can be easily modified to other cases of interest by changing accordingly the coefficients $\alpha_{1,2}$ in (7) (depending on terminations/lumped loads) and $Y_{g1,2}$ in the local model formalism (11)–(14).

In Section II, we will present several numerical examples to validate the proposed local thickness-dependent permittivity model for far-field and near-field excitation problems. The nonlocal model for WM structures (which requires the ABCs at wire terminations) have been extensively verified in the literature [7]–[12], [15]–[24], [26]–[29], [37], [40], among others, versus full-wave numerical simulations for a variety of scattering, excitation, and radiation problems involving wire media, and can be used for an adequate comparison with the local thickness-dependent permittivity model results. Also, we will demonstrate that the homogenized local WM can be effectively used in the full-wave numerical simulator to significantly reduce the computation time and memory in the analysis of true physical WM structures. Once the accuracy of our model has been established, its usefulness compared to both the nonlocal model (necessitating ABCs, and restricted to canonical planar geometries) and full-wave solvers should be clear.

III. Numerical Results and Discussions

In the first numerical example we consider a mushroom-type high-impedance surface with lumped impedance insertions at the connection of the vias to the ground plane with the geometry shown in Fig. 3. The response of the structure with the TM-polarized plane-wave incidence has been studied in [37] based on the nonlocal homogenization model.

The local thickness-dependent permittivity model is utilized with $\alpha_1 = C_p/C_w$ and $\alpha_2 = (j\omega C_w Z_{\text{load eff}})^{-1}$ in (7). The reflection coefficient is obtained by solving either (11) or (12), or directly using (13) (with $L/2$ replaced by L) corresponding to the equivalent geometry in Fig. 2. The results for the phase of the reflection coefficient with different values of inductive and capacitive loads (including the cases of open circuit (OC) and short circuit (SC) vias) are shown in Fig. 4 and compared with the exact nonlocal results and full-wave numerical simulations using HFSS from [37], demonstrating good agreement with the previously obtained results.

As pointed out in Section II, the local thickness-dependent permittivity (7) takes into account SD in WM in the averaged sense per thickness of the WM slab and the effect of the loads/terminations. Fig. 5 shows the frequency dispersion of the local permittivity for a WM with the vias connected to the metallic patches at $z = 0$ and to the ground plane through the lumped inductive or capacitive loads at $z = -L$ (Fig. 3). The values of the loads and the dimensions of the structure are as in Fig. 4. It can be seen that the local permittivity depends on the type and the value of the load and resonates at the Fabry–Pérot (FP) condition associated with the effective thickness of the WM slab, resulting in extremely large values of the local permittivity. We should point out that for a fixed L and very long wavelength and in the static limit the local permittivity (7) does not reduce to the host permittivity ε_h and it strongly depends on the lumped loads and wire terminations. It can be seen in Fig. 5(b) for the cases of SC and inductive lumped insertions that the local permittivity (7) has very large *positive* values in the limit of frequency approaching zero. We should also point out that for a typical scenario of a mushroom structure (with SC wires in this case) considered in the literature (see [9]), wherein the conclusion was about the suppression of SD by the presence of patches at the wire connection such that the local Drude (bulk) permittivity is valid in this case, this is not true at low frequencies (as the Drude model predicts a *negative* permittivity at low frequencies). In the quasi-static limit SD in WM structures is strongly pronounced and it is taken into account by the local thickness-dependent permittivity (7). The local permittivity (7) turns to the local Drude (bulk) permittivity only if SD effects are completely suppressed at all the frequencies, including the static limit.

The local thickness-dependent permittivity (7) reduces to the host permittivity ε_h only in the limit of $L \to 0$ such that for a sufficiently small frequency $k_h L \to 0$ and $\varepsilon_{\text{loc}} \to \varepsilon_h$.

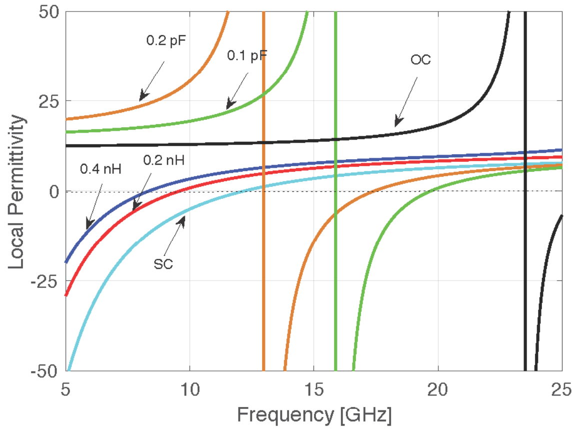

(a)

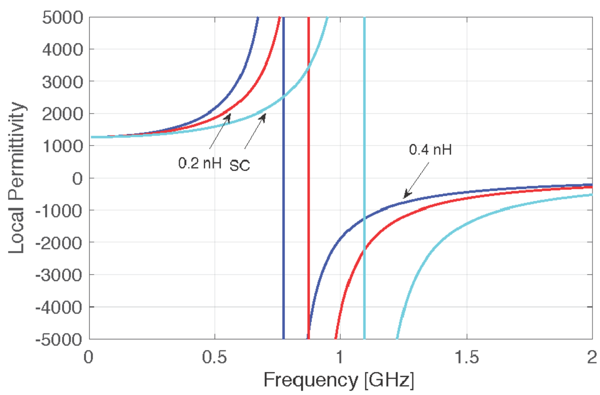

(b)

Fig. 5. (a) Local thickness-dependent permittivity of the WM slab with the vias connected to the metallic patches and to the ground plane through the lumped loads and (b) same at low frequencies for the cases with SC and inductive lumped loads demonstrating very large values of the local permittivity even in the static limit. The various lumped loads correspond to those in Fig. 4.

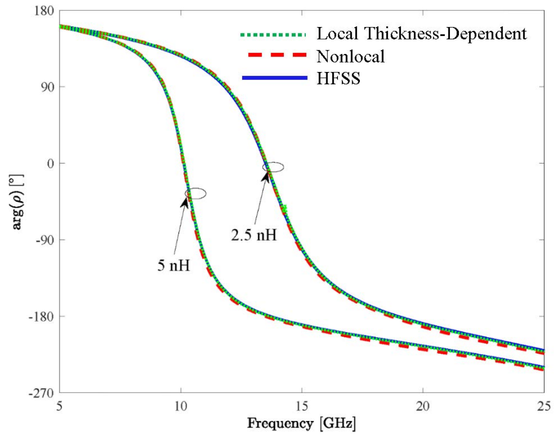

Fig. 6. Phase of the reflection coefficient for the air-filled mushroom structure with the vias connected to the ground plane through inductive loads (2.5 and 5 nH) (with the geometry in Fig. 3). The dimensions of the structure are: $a = 2$ mm, $g = 0.2$ mm, $r_0 = 0.05$ mm, $L = 1$ mm, $\varepsilon_h = 1$, and $\theta_i = 45°$.

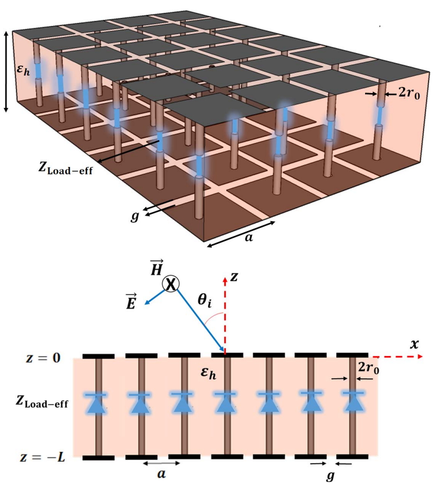

Fig. 7. Geometry of a two-sided mushroom structure with the vias connected to p-i-n diodes with an obliquely incident TM-polarized plane wave.

The results in Fig. 5 show that at some frequencies the local thickness-dependent permittivity is zero. This results in a singularity of the propagation constant along the wires in the local model $\gamma_{\text{loc}} = \sqrt{(\varepsilon_h k_x^2/\varepsilon_{\text{loc}}) - k_h^2}$ leading to a rapid variation in phase and spurious resonances in the reflection phase in a very narrow frequency band. The spurious resonances are highly sensitive to small perturbations (for example, they vanish for small dielectric loss in the host permittivity). The issue of spurious resonances in the local model has been discussed in [9].

In Fig. 6, the reflection-phase characteristics are shown for an air-filled mushroom structure with the vias connected to inductive loads of a large value, and the results are compared with the nonlocal solution and the full-wave numerical simulations from [37], demonstrating nearly perfect agreement. The effects of the parasitic inductance and parasitic capacitance are negligible in such a case of an air-filled structure. It should be noted that the local thickness-dependent permittivity model accurately captures the response of the structure even with large discrete lumped loads.

In the second numerical example, we consider a two-sided mushroom structure (with the same patch arrays at the WM interfaces) with the vias connected to p-i-n diodes in the middle of the structure (with the geometry shown in Fig. 7). This structure has been studied in [40] using a nonlocal homogenization model.

The local thickness-dependent permittivity model has been applied in the analysis of the structure due to the obliquely incident TM-polarized plane wave. Because of the symmetry of the structure, even and odd excitations can be used with $\alpha_1 = C_p/C_w$ and $\alpha_2 = (j\omega C_w Z_{\text{diode eff}})^{-1}$ in the PEC symmetry in (7), and with $\alpha_1 = C_p/C_w$ and $\alpha_2 = 0$ in the PMC symmetry in (7). The response of the structure is obtained with (13) and (14) (for the equivalent problem in Fig. 2). The p-i-n diodes are modeled as effective diode loads with the impedance of diodes in the ON and OFF states as the series connection of lumped resistors and capacitors with $R = 3$ Ohms and $C = 0.025$ pF. The diodes are inserted in the vias through a gap of 0.73 mm. The parasitic loads in order to characterize the gap were estimated with the values of the parasitic capacitance of $C_{\mathrm{par}} \approx 0.02$ pF and the parasitic inductance of $L_{\mathrm{par}} \approx 0.1$ nH [40].

The results of the transmission coefficient (magnitude and phase) based on the local thickness-dependent permittivity formalism are shown in Fig. 8 for both OFF [see Fig. 8(a) and (b)] and ON [Fig. 8(c) and (d)] states and compared with the nonlocal and CST MWS results from [40], demonstrating great agreement.

Next, we validate the proposed local thickness-dependent permittivity model for near-field excitation, with a specific application to subwavelength imaging problems involving WM-type lenses. First, we consider a WM slab with the magnetic line source excitation (with the geometry shown in Fig. 9). The transmission coefficient for propagating and evanescent waves from the source is calculated either by (11) or (12), or with the even and odd excitation (due to symmetry of the structure) using (13) and (14) with $\alpha_1 = \alpha_2 = 0$ in (7) (see Fig. 2 for an equivalent problem). Then, the magnetic field at the image plane at a distance z from the lower interface of the WM slab is calculated as a numerical solution of the Sommerfeld integral in the spectral domain [23]

$$H_y(x) = \frac{I_0 k_0^2}{j\pi\omega\mu_0} \int_0^{\infty} \frac{1}{2\gamma_0} e^{-\gamma_0(2d)} T(\omega, k_x) \cos(k_x x) dk_x. \quad (15)$$

The response of the WM slab to evanescent waves from the source is studied based on the local thickness-dependent permittivity model and compared with the nonlocal homogenization model results in Fig. 10 (with the nonlocal model formulation from [11]).

The square normalized amplitude of the magnetic-field profile at the image plane as a function of x/λ at the operating frequency of 19 THz is calculated as a numerical solution of (15) for both local thickness-dependent permittivity model and nonlocal model and shown in Fig. 11. It is assumed that the magnetic line source and the image plane are located at $d = 150$ nm. Good agreement is observed between local and nonlocal results.

We follow-up with the example of a WM slab loaded with a 2-D material (such as a graphene) at the WM interfaces and excited by a magnetic line source (with the geometry shown in Fig. 12). The nonlocal homogenization model and the numerical results with the line source excitation have been presented in [24]. The transmission response of the structure based on the local thickness-dependent permittivity formalism is obtained for propagating and evanescent waves from the source either by (11) or (12), or using the even and odd excitation (13) and (14) with $\alpha_1 = \alpha_2 = \sigma_s / j\omega\varepsilon_0\varepsilon_h$ in (7) (see Fig. 2 for an equivalent problem), where σ_s is the complex surface conductivity of graphene modeled with the Kubo formula [41].

The response of the graphene loaded WM slab to evanescent waves is shown in Fig. 13 based on the local thickness-dependent permittivity model and compared with the nonlocal homogenization model results from [24], demonstrating good agreement.

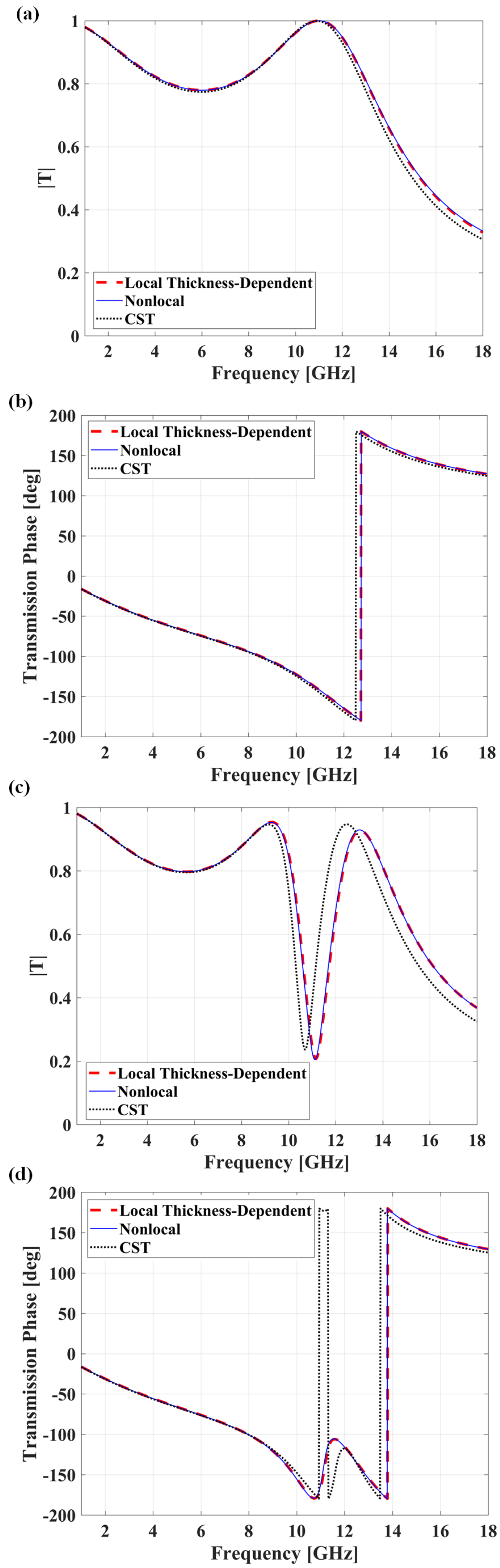

Fig. 8. Transmission response (magnitude and phase) of the two-sided mushroom structure with the vias connected to p-i-n diodes in the middle of the WM slab in (a) and (b) OFF, and (c) and (d) ON states under illumination of an obliquely incident TM-polarized plane wave. The dimensions of the structure are: $a = 2$ mm, $g = 0.2$ mm, $r_0 = 0.05$ mm, $L = 2$ mm, $\varepsilon_h = 10.2$, and $\theta_i = 60°$.

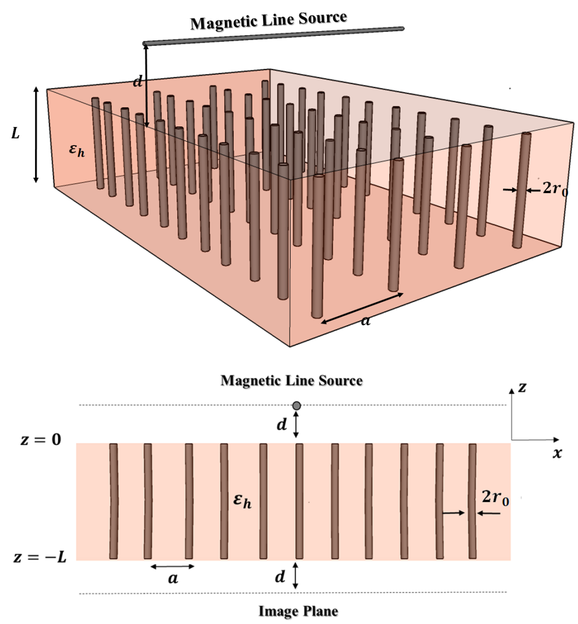

Fig. 9. Geometry of a WM slab excited by a magnetic line source.

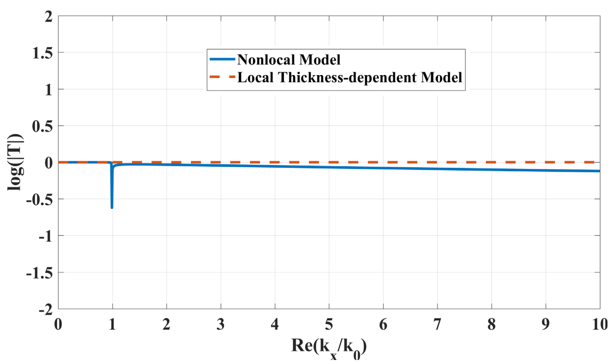

Fig. 10. Transmission response (in logarithmic units) of a WM slab for evanescent waves excited by a magnetic line source. The dimensions of the structure are: $a = 215$ nm, $r_0 = 21.5$ nm, $L = 7894$ nm, and $\varepsilon_h = 1$.

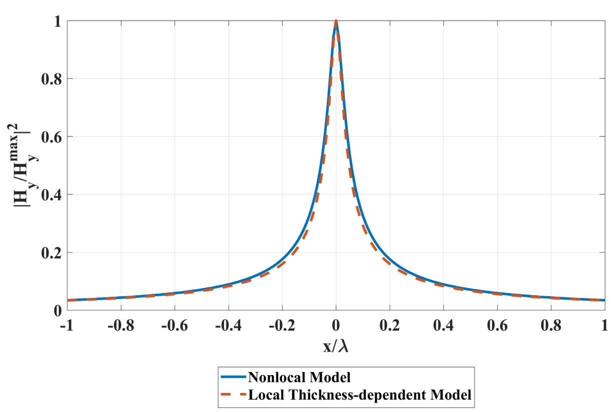

Fig. 11. Square normalized amplitude of the magnetic field at the image plane as a function of x/λ at the operating frequency of 19 THz for a WM slab excited by a magnetic line source.

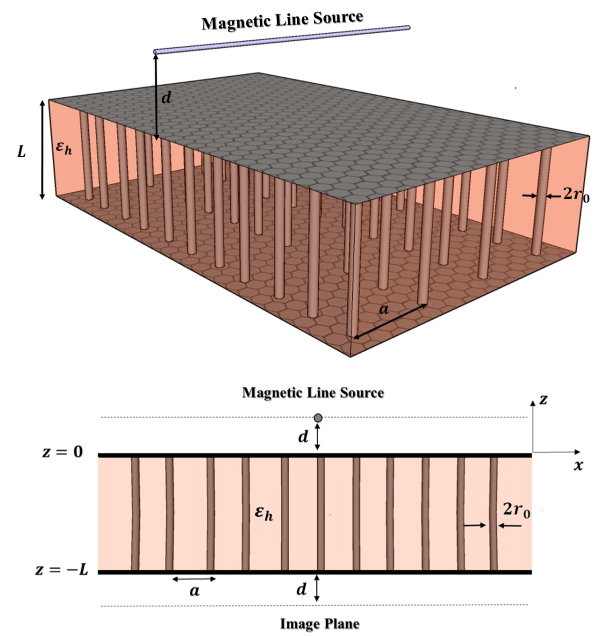

Fig. 12. Geometry of a WM slab loaded by graphene sheets at the WM interfaces and excited by a magnetic line source.

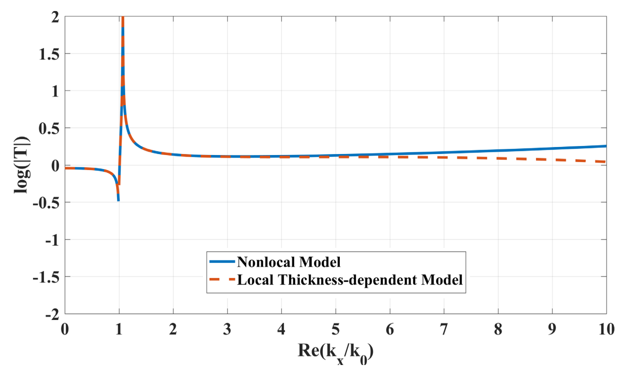

Fig. 13. Transmission response (in logarithmic units) of a WM slab loaded with graphene sheets for the evanescent waves due to a magnetic line source excitation. The dimensions of the WM slab and graphene parameters are: $a = 215$ nm, $r_0 = 21.5$ nm, $L = 2400$ nm, $\varepsilon_h = 1$, $T = 300$ K, $\tau = 0.5$ ps, and $\mu_c = 1.5$ eV.

The square normalized amplitude of the magnetic field at the image plane as a function of x/λ at the operating frequency of 19 THz is shown in Fig. 14 by numerically integrating (15) with the known expression for the transmission coefficient (based on the local and nonlocal homogenization models). The location of the magnetic line source and the image plane is the same as in the previous example, $d = 150$ nm. The results of both analytical models are in very good agreement.

In the final examples, the obtained analytical expression (7) for the local thickness-dependent permittivity of WM has been used in the full-wave numerical simulator CST Microwave Studio [42]. The WM slab is modeled in CST MWS as a uniform local anisotropic material with the host permittivity in the x- and y-directions and the local thickness-dependent permittivity along the z-direction (see Fig. 2 for an equivalent problem). This significantly reduces the computation time and memory when modeling true physical WM structures. The examples of a WM slab and WM slab loaded with graphene

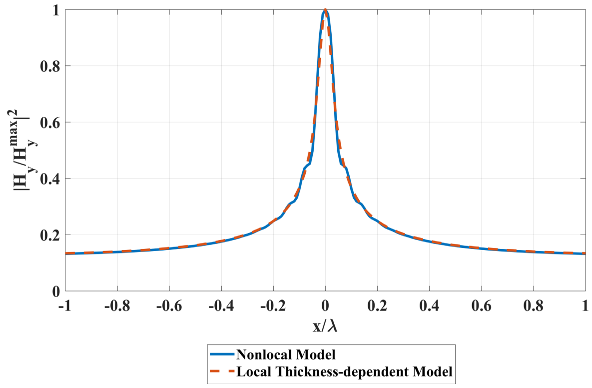

Fig. 14. Square normalized amplitude of the magnetic field at the image plane as a function of x/λ at the operating frequency of 19 THz for a WM slab loaded with graphene sheets at the WM interfaces and excited by a magnetic line source.

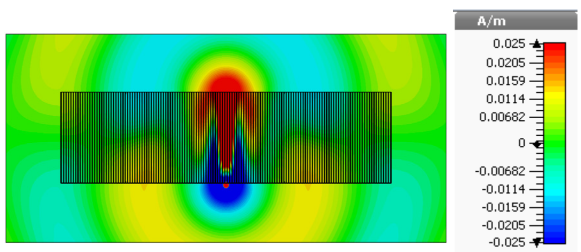

(a)

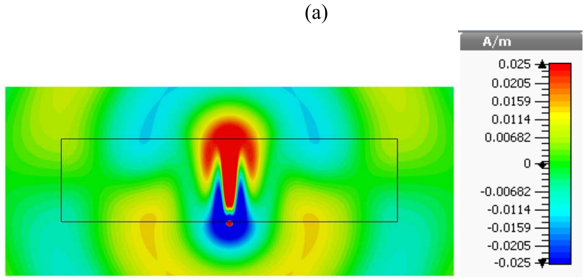

(b)

Fig. 15. Numerical simulations of the magnetic-field distribution for (a) true physical WM slab and (b) homogenized local anisotropic material excited by a magnetic line source.

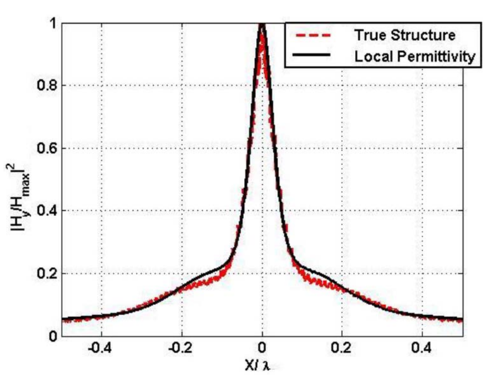

Fig. 16. Square normalized amplitude of the magnetic field at the image plane for a true physical WM slab and homogenized local anisotropic slab excited by a magnetic line source.

sheets at the interfaces and excited by a magnetic line source considered above are included here to demonstrate the idea of using a homogenized material in the full-wave simulator.

TABLE I

COMPARISON OF COMPUTATION TIME AND MEMORY IN CST SIMULATIONS FOR A WM SLAB EXCITED BY A MAGNETIC LINE SOURCE

Structure	Time (minutes)	Mesh Cells (millions)
True WM slab	35	5.703
Local permittivity model	8	1.139

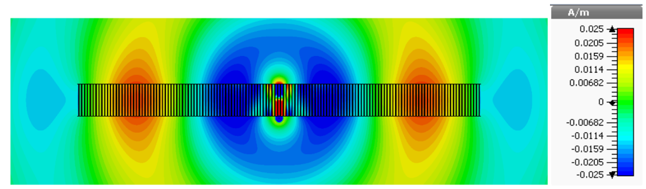

(a)

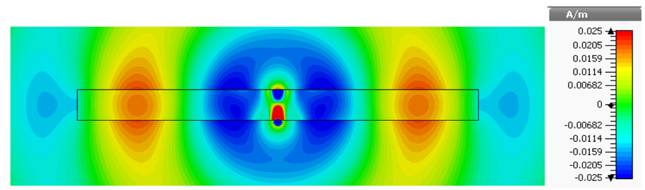

(b)

Fig. 17. Numerical simulations of the magnetic-field distribution for (a) true physical WM slab loaded with graphene sheets and (b) homogenized local anisotropic material loaded with graphene sheets and excited by a magnetic line source.

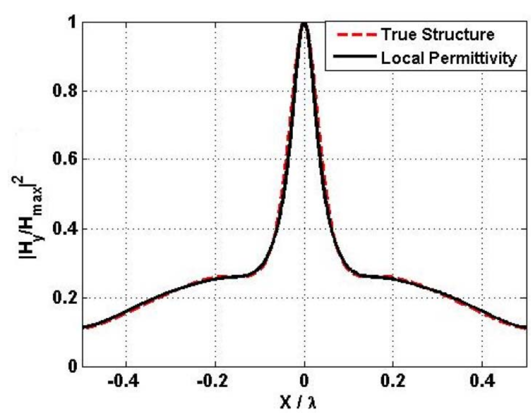

Fig. 18. Square normalized amplitude of the magnetic field at the image plane for a true physical WM slab with graphene sheets and homogenized local anisotropic slab with graphene sheets excited by a magnetic line source.

The same dimensions are used for WM and parameters of graphene as in the previous examples (see Figs. 9 and 12). In Fig. 15, for the case of a WM slab excited by a magnetic line source (see Fig. 9), the magnetic-field distribution is shown for homogenized and true physical structures, with the results for the square normalized amplitude of the magnetic field at the image plane demonstrated in Fig. 16.

The same accuracy of 250 mesh cells per wavelength are used in both simulations for homogenized and true physical WM slab. Table I documents the simulation time and the number of mesh cells used in the CST MWS simulations.

TABLE II
COMPARISON OF COMPUTATION TIME AND MEMORY IN CST SIMULATIONS FOR A WM SLAB LOADED WITH GRAPHENE SHEETS AND EXCITED BY A MAGNETIC LINE SOURCE

Structure	Time (minutes)	Mesh Cells (millions)
True WM slab	38	7.604
Local permittivity model	17	3.245

The numerical simulation results for the magnetic-field distribution for the example of a WM slab loaded with graphene sheets at the interfaces (see Fig. 12) are shown in Fig. 17 for homogenized and true physical structures.

The simulation results for the square normalized amplitude of the magnetic field at the image plane are shown in Fig. 18. The same accuracy of 200 mesh cells per wavelength is used in both simulations for homogenized and true physical structures. Table II [33] documents the simulation time and the number of mesh cells used in the CST MWS simulations.

IV. CONCLUSION

A local thickness-dependent permittivity model has been proposed for a general case of a WM structure with the wires connected to impedance surfaces through lumped impedance insertions. A closed-form expression of a local thickness-dependent permittivity has been derived which takes into account SD in WM in the average sense per thickness of the WM slab and the effect of lumped loads and impedance surface terminations. The local model necessitates the solution for the nonlocal permittivity in the spatial domain; however, once it is derived, it enables to obtain a general closed-form expression for the local thickness-dependent permittivity, which simplifies the formulation for various geometrically complex excitation and scattering problems involving WM. In the local framework, the WM slab with lumped impedance insertions and terminated with impedance surfaces is replaced by a local uniaxial anisotropic material subject to traditional boundary conditions at the interfaces (without the need for ABCs required in the nonlocal model). It is demonstrated with various numerical examples that the local permittivity framework provides accurate solutions for far-field and near-field electromagnetic problems. In general, the proposed theory captures accurately the nonlocal wave dynamics of the WM for metamaterial slabs with electrically short wires, $k_h L \leq 1$ and $L \leq a$. For long wires, $L/a \gg 1$, the model is accurate at low frequencies when the WM behaves as the material with extreme anisotropy, or when the wires are densely packed, $a/L \ll 1$, and not necessarily electrically short, so that the plasma frequency is extremely large.

We have also introduced the local thickness-dependent permittivity in the full-wave numerical simulator CST Microwave Studio and have demonstrated a significant reduction of computation time and memory when modeling true physical WM structures as homogenized anisotropic materials.

Moreover, the theory highlights that the dependence of the effective permittivity of "local" models on the material thickness, which is a feature common to most metamaterials, is a consequence of a nonlocal electromagnetic response.

APPENDIX
GREEN'S FUNCTION PROBLEM

For a general case of a WM structure shown in Fig. 1 the Green's function problem is formulated for the wave equation (3) subject to the ABCs at the wire-end connections at $z = 0$ and $z = -L$ [25]–[29]

$$\left(\frac{\partial^2}{\partial z^2} + k_h^2\right) g(z, z') = -\delta(z - z') \tag{16}$$

$$\left[g(z, z') + \alpha_1 \frac{\partial g(z, z')}{\partial z}\right]\Bigg|_{z=0} = 0 \tag{17}$$

$$\left[g(z, z') - \alpha_2 \frac{\partial g(z, z')}{\partial z}\right]\Bigg|_{z=-L} = 0. \tag{18}$$

The solution of the boundary-value problem (16)–(18) is obtained as follows:

$$g(z, z') = \frac{e^{-jk_h|z-z'|}}{2jk_h} - \frac{e^{-jk_h(z-z')}}{2jk_h} + \left(e^{jk_h z} - e^{-jk_h z}\frac{1 + jk_h\alpha_1}{1 - jk_h\alpha_1}\right) B(z') \tag{19}$$

where $\mathrm{B}(z')$ is given at the bottom of this page as (20).

In (19) and (20), α_1 and α_2 depend on the lumped impedance insertions and impedance surface terminations, such that for lumped loads attached to metallic patches

$$\alpha_1 = \left(j\omega C_w Z_{\text{load eff1}} + \frac{C_w}{C_{p1}}\right)^{-1}$$
$$\alpha_2 = \left(j\omega C_w Z_{\text{load eff2}} + \frac{C_w}{C_{p2}}\right)^{-1} \tag{21}$$

and for lumped loads connected to thin metal/2-D material

$$\alpha_1 = \left(j\omega C_w Z_{\text{load eff1}} + \frac{j\omega\varepsilon_0\varepsilon_h}{\sigma_{s1}}\right)^{-1}$$
$$\alpha_2 = \left(j\omega C_w Z_{\text{load eff2}} + \frac{j\omega\varepsilon_0\varepsilon_h}{\sigma_{s2}}\right)^{-1}. \tag{22}$$

Here, $Z_{\text{load eff1,2}}$ are defined in [23], [28], and [37], and C_w and $C_{p1,2}$ are given in [43], and $\sigma_{s1,2}$ determines a complex surface conductivity of 2-D material.

ACKNOWLEDGMENT

The authors would like to thank A. Forouzmand for his help regarding the validation of local thickness-dependent permittivity model for near-field excitation and G. Moreno for helping with CST Microwave Studio simulations.

$$B(z') = \frac{1 - jk_h\alpha_1}{2jk_h} \frac{e^{jk_h(z'+L)}(1 + jk_h\alpha_2) - e^{-jk_h(z'+L)}(1 - jk_h\alpha_2)}{e^{-jk_h L}(1 - jk_h\alpha_1)(1 - jk_h\alpha_2) - e^{jk_h L}(1 + jk_h\alpha_1)(1 + jk_h\alpha_2)} \tag{20}$$

REFERENCES

[1] L. D. Landau, E. M. Lifshitz, and L. P. Pitaevskii, *Electrodynamics of Continuous Media*, vol. 8, 2nd ed. Oxford, U.K.: Elsevier Butterworth-Heinemann, 1984.

[2] V. M. Agranovich and V. Ginzburg, *Crystal Optics with Spatial Dispersion, and Excitons*, 2nd ed. Berlin, Germany: Springer-Verlag, 1984.

[3] P. Halevi Ed., *Spatial Dispersion in Solids and Plasmas*, Amsterdam, The Netherlands: North-Holland, 1992, pp. 350–367, ch. 6.

[4] F. Forstmann and R. R. Gerhardts, *Metal Optics Near the Plasma Frequency*. Berlin, Germany: Springer, 1982.

[5] G. Shvets, "Photonic approach to making a surface wave accelerator," in *Proc. 10th Adv. Accel. Concepts Workshop*, vol. 647, Nov. 2002, pp. 371–382.

[6] P. A. Belov *et al.*, "Strong spatial dispersion in wire media in the very large wavelength limit," *Phys. Rev. B, Condens. Matter*, vol. 67, Mar. 2003, Art. no. 113103.

[7] M. G. Silveirinha and C. A. Fernandes, "Homogenization of 3-D-connected and nonconnected wire metamaterials," *IEEE Trans. Microw. Theory Techn.*, vol. 53, no. 4, pp. 1418–1430, Apr. 2005.

[8] M. G. Silveirinha, C. A. Fernandes, and J. R. Costa, "Electromagnetic characterization of textured surfaces formed by metallic pins," *IEEE Trans. Antennas Propag.*, vol. 56, no. 2, pp. 405–415, Feb. 2008.

[9] O. Luukkonen, M. G. Silveirinha, A. B. Yakovlev, C. R. Simovski, I. S. Nefedov, and S. A. Tretyakov, "Effects of spatial dispersion on reflection from mushroom-type artificial impedance surfaces," *IEEE Trans. Microw. Theory Techn.*, vol. 57, no. 11, pp. 2692–2699, Nov. 2009.

[10] A. B. Yakovlev, M. G. Silveirinha, O. Luukkonen, C. R. Simovski, I. S. Nefedov, and S. A. Tretyakov, "Characterization of surface-wave and leaky-wave propagation on wire-medium slabs and mushroom structures based on local and nonlocal homogenization models," *IEEE Trans. Microw. Theory Techn.*, vol. 57, no. 11, pp. 2700–2714, Nov. 2009.

[11] P. A. Belov and M. G. Silveirinha, "Resolution of subwavelength transmission devices formed by a wire medium," *Phys. Rev. E, Stat. Phys. Plasmas Fluids Relat. Interdiscip. Top.*, vol. 73, May 2006, Art. no. 056607.

[12] M. G. Silveirinha, P. A. Belov, and C. R. Simovski, "Subwavelength imaging at infrared frequencies using an array of metallic nanorods," *Phys. Rev. B, Condens. Matter*, vol. 75, Jan. 2007, Art. no. 035108.

[13] P. Burghignoli, G. Lovat, F. Capolino, D. R. Jackson, and D. R. Wilton, "Modal propagation and excitation on a wire-medium slab," *IEEE Trans. Microw. Theory Techn.*, vol. 56, no. 5, pp. 1112–1124, May 2008.

[14] P. Burghignoli, G. Lovat, F. Capolino, D. R. Jackson, and D. R. Wilton, "Directive leaky-wave radiation from a dipole source in a wire-medium slab," *IEEE Trans. Antennas Propag.*, vol. 56, no. 5, pp. 1329–1339, May 2008.

[15] M. G. Silveirinha, "Broadband negative refraction with a crossed wire mesh," *Phys. Rev. B, Condens. Matter*, vol. 79, Apr. 2009, Art. no. 153109.

[16] M. G. Silveirinha and A. B. Yakovlev, "Negative refraction by a uniaxial wire medium with suppressed spatial dispersion," *Phys. Rev. B, Condens. Matter*, vol. 81, no. 23, Jun. 2010, Art. no. 233105.

[17] C. S. R. Kaipa, A. B. Yakovlev, S. I. Maslovski, and M. G. Silveirinha, "Indefinite dielectric response and all-angle negative refraction in a structure with deeply-subwavelength inclusions," *Phys. Rev. B, Condens. Matter*, vol. 84, no. 16, Oct. 2011, Art. no. 165135.

[18] M. G. Silveirinha and S. I. Maslovski, "Radiation from elementary sources in a uniaxial wire medium," *Phys. Rev. B, Condens. Matter*, vol. 85, Apr. 2012, Art. no. 155125.

[19] G. W. Hanson, E. Forati, and M. G. Silveirinha, "Modeling of spatially-dispersive wire media: Transport representation, comparison with natural materials, and additional boundary conditions," *IEEE Trans. Antennas Propag.*, vol. 60, no. 9, pp. 4219–4232, Sep. 2012.

[20] E. Forati and G. W. Hanson, "Scattering from isotropic connected wire medium metamaterials: Three-, two-, and One-dimensional cases," *IEEE Trans. Antennas Propag.*, vol. 61, no. 7, pp. 3564–3574, Jul. 2013.

[21] E. Forati and G. W. Hanson, "Transport model for homogenized uniaxial wire media: Three-dimensional scattering problems and homogenized model limits," *Phys. Rev. B, Condens. Matter*, vol. 88, Sep. 2013, Art. no. 125125.

[22] Y. R. Padooru *et al.*, "New absorbing boundary conditions and analytical model for multilayered mushroom-type metamaterials: Applications to wideband absorbers," *IEEE Trans. Antennas Propag.*, vol. 60, no. 12, pp. 5727–5742, Dec. 2012.

[23] C. S. R. Kaipa, A. B. Yakovlev, M. G. Silveirinha, and S. I. Maslovski, "Near-field imaging with a loaded wire medium," *Phys. Rev. B, Condens. Matter*, vol. 86, Oct. 2012, Art. no. 155103.

[24] A. Forouzmand, H. M. Bernety, and A. B. Yakovlev, "Graphene-loaded wire medium for tunable broadband subwavelength imaging," *Phys. Rev. B, Condens. Matter*, vol. 92, Aug. 2015, Art. no. 085402.

[25] G. W. Hanson, M. G. Silveirinha, P. Burghignoli, and A. B. Yakovlev, "Non-local susceptibility of the wire medium in the spatial domain considering material boundaries," *New J. Phys.*, vol. 15, Aug. 2013, Art. no. 083018.

[26] M. G. Silveirinha, "Additional boundary condition for the wire medium," *IEEE Trans. Antennas Propag.*, vol. 54, no. 6, pp. 1766–1780, Jun. 2006.

[27] M. G. Silveirinha, C. A. Fernandes, and J. R. Costa, "Additional boundary condition for a wire medium connected to a metallic surface," *New J. Phys.*, vol. 10, May 2008, Art. no. 053011.

[28] S. I. Maslovski, T. A. Morgado, M. G. Silveirinha, C. S. R. Kaipa, and A. B. Yakovlev, "Generalized additional boundary conditions for wire media," *New J. Phys.*, vol. 12, Nov. 2010, Art. no. 113047.

[29] A. B. Yakovlev, Y. R. Padooru, G. W. Hanson, A. Mafi, and S. Karbasi, "A generalized additional boundary condition for mushroom-type and bed-of-nails-type wire media," *IEEE Trans. Microw. Theory Techn.*, vol. 59, no. 3, pp. 527–532, Mar. 2011.

[30] A. B. Yakovlev, M. Hedayati, M. G. Silveirinha, and G. W. Hanson, "Local thickness-dependent permittivity model for nonlocal bounded wire-medium structures," *Phys. Rev. B, Condens. Matter*, vol. 94, Oct. 2016, Art. no. 155442.

[31] C. R. Simovski, "On electromagnetic characterization and homogenization of nanostructured metamaterials," *J. Opt.*, vol. 13, no. 1, Nov. 2010, Art. no. 013001.

[32] Y. Luo, A. I. Fernandez-Dominguez, A. Wiener, S. A. Maier, and J. B. Pendry, "Surface plasmons and nonlocality: A simple model," *Phys. Rev. Lett.*, vol. 111, Aug. 2013, Art. no. 093901.

[33] G. Moreno, M. Hedayati, A. Forouzmand, A. B. Yakovlev, M. G. Silveirinha, and G. W. Hanson, "Local thickness-dependent permittivity of wire media in CST Microwave Studio," in *Proc. IEEE Int. Symp. Antennas Propag. USNC/URSI Nat. Radio Sci. Meeting*, Jul. 2017, pp. 1957–1958.

[34] G. Moreno, A. Forouzmand, A. B. Yakovlev, M. G. Silveirinha, and G. W. Hanson, "Systematic development of a robust circuit-model technique for subwavelength imaging with wire-medium type lenses," in *Proc. IEEE Int. Symp. Antennas Propag. USNC/URSI Nat. Radio Sci. Meeting*, Jul. 2017, pp. 1953–1954.

[35] A. B. Yakovlev, "Nonlocality of wire media—Local thickness-dependent permittivity model," in *Proc. 11th Int. Congr. Engineered Mater. Platforms Novel Wave Phenomena (Metamaterials)*, Marseille, France, Sep. 2017, pp. 379–381.

[36] O. Luukkonen *et al.*, "Simple and accurate analytical model of planar grids and high-impedance surfaces comprising metal strips or patches," *IEEE Trans. Antennas Propag.*, vol. 56, no. 6, pp. 1624–1632, Jun. 2008.

[37] C. S. R. Kaipa, A. B. Yakovlev, S. I. Maslovski, and M. G. Silveirinha, "Mushroom-type high-impedance surface with loaded vias: Homogenization model and ultra-thin design," *IEEE Antennas Wireless Propag. Lett.*, vol. 10, pp. 1503–1506, 2011.

[38] D. M. Pozar, *Microwave Engineering*, 4th ed. Hoboken, NJ, USA: Wiley, 2011.

[39] F. Medina, F. Mesa, and D. C. Skigin, "Extraordinary transmission through arrays of slits: A circuit theory model," *IEEE Trans. Microw. Theory Techn.*, vol. 58, no. 1, pp. 105–115, Jan. 2010.

[40] A. Forouzmand, C. S. R. Kaipa, and A. B. Yakovlev, "Mushroom-type structures with the wires connected through diodes: Theory and applications," *J. Appl. Phys.*, vol. 120, Jul. 2016, Art. no. 015303.

[41] G. W. Hanson, "Dyadic Greens functions and guided surface waves on graphene," *J. Appl. Phys.*, vol. 103, Jan. 2008, Art. no. 064302.

[42] (2015). *CST Microwave Studio*. [Online]. Available: www.cst.com

[43] S. I. Maslovski and M. G. Silveirinha, "Nonlocal permittivity from a quasistatic model for a class of wire media," *Phys. Rev. B, Condens. Matter*, vol. 80, Dec. 2009, Art. no. 245101.

Alexander B. Yakovlev (S'94–M'97–SM'01) received the Ph.D. degree in radiophysics from the Institute of Radiophysics and Electronics, National Academy of Sciences, Kharkiv, Ukraine, in 1992, and the Ph.D. degree in electrical engineering from the University of Wisconsin–Milwaukee, Milwaukee, WI, USA, in 1997.

In 2000, he joined the Department of Electrical Engineering, The University of Mississippi, Oxford, MS, USA, as an Assistant Professor, and became an Associate Professor in 2004. Since 2013, he has been a Full Professor of electrical engineering with The University of Mississippi. He is the coauthor of the book *Operator Theory for Electromagnetics: An Introduction* (Springer, New York, NY, USA, 2002). His current research interests include mathematical methods in applied electromagnetics, homogenization theory, high-impedance surfaces for antenna applications, electromagnetic band-gap structures, metamaterial structures, wire media, graphene, cloaking, the theory of leaky waves, transient fields in layered media, and catastrophe and bifurcation theories.

Dr. Yakovlev is a member of the URSI Commission. He received the Young Scientist Award from the 1992 URSI International Symposium on Electromagnetic Theory, Sydney, NSW, Australia, and the Young Scientist Award from the 1996 International Symposium on Antennas and Propagation, Chiba, Japan. In 2003, he received the Junior Faculty Research Award, the Faculty Teaching Award in 2017, the Senior Faculty Research Award in 2018, and the Outstanding Faculty Member of the Year Award from the School of Engineering, The University of Mississippi, in 2019. From 2003 to 2006, he was an Associate Editor-in-Chief of the *Applied Computational Electromagnetics Society (ACES) Journal*. He was an Associate Editor of the IEEE TRANSACTIONS ON MICROWAVE THEORY AND TECHNIQUES from 2005 to 2008. Since 2017, he has been an Associate Editor of the IEEE ANTENNAS AND WIRELESS PROPAGATION LETTERS. He is currently an Associate Editor of the IEEE TRANSACTIONS ON ANTENNAS AND PROPAGATION.

Mário G. Silveirinha (S'99–M'03–SM'13–F'14) received the Licentiate degree in electrical engineering from the University of Coimbra, Coimbra, Portugal, in 1998, and the Ph.D. degree in electrical and computer engineering (with a minor in applied mathematics) from the Instituto Superior Técnico (IST), Technical University of Lisbon, Lisbon, Portugal, in 2003.

He is currently a Professor with IST, University of Lisbon, Lisbon, and a Senior Researcher with Instituto de Telecomunicações, Lisbon. His current research interests include electromagnetism, plasmonics and metamaterials, quantum optics, and topological effects.

Dr. Silveirinha is an IEEE Fellow 2014 with the citation for contributions to the electrodynamics of metamaterials. He is a Junior Member of the Academy of Sciences of Lisbon, Lisbon. He was a 2018 recipient of the IET Harvey Engineering Research Prize for contributions to electrodynamics of metamaterials and its applications to microwave components and devices.

George W. Hanson (S'85–M'91–SM'98–F'09) was born in Glen Ridge, NJ, USA, in 1963. He received the B.S.E.E. degree from Lehigh University, Bethlehem, PA, USA, in 1986, the M.S.E.E. degree from Southern Methodist University, Dallas, TX, USA, 1988, and the Ph.D. degree from Michigan State University, East Lansing, East Lansing, MI, USA, in 1991.

From 1986 to 1988, he was a Development Engineer with General Dynamics, Fort Worth, TX, where he was involved in radar simulators. From 1988 to 1991, he was a Research and Teaching Assistant with the Department of Electrical Engineering, Michigan State University. He is currently a Professor of electrical engineering and computer science with the University of Wisconsin–Milwaukee, Milwaukee, WI, USA. He is the coauthor of the book *Operator Theory for Electromagnetics: An Introduction* (Springer, NY, USA, 2002) and the author of *Fundamentals of Nanoelectronics* (Prentice-Hall, NJ, USA, 2007). His current research interests include nanoelectromagnetics, quantum optics, mathematical methods in electromagnetics, and electromagnetic wave phenomena in layered media.

Dr. Hanson is a member of the URSI Commission B, Sigma Xi, and Eta Kappa Nu. In 2006, he received the S. A. Schelkunoff Best Article Award from the IEEE Antennas and Propagation Society. He was an Associate Editor of the IEEE TRANSACTIONS ON ANTENNAS AND PROPAGATION from 2002 to 2007.